Optical properties of hexagonal boron nitride

A. Zunger*
Department of Theoretical Physics, Soreq Nuclear Research Centre, Yavne, Israel and Department of Chemistry, Tel Aviv University, Tel Aviv, Israel

A. Katzir
Department of Solid State Physics, Soreq Nuclear Research Centre, Yavne, Israel

A. Halperin
The Racah Institute of Physics, The Hebrew University, Jerusalem, Israel
(Received 16 June 1975)

Optical absorption, reflectivity, and photoconductivity in the near-uv range (1950–3200 Å) of a thin film of hexagonal boron nitride were measured. The main absorption peak was observed at 6.2 eV. A sharp fall at about 5.8 eV was attributed to the direct band gap. The temperature dependence of the band gap was found to be less than 4×10^{-5} eV/°K. Self-consistent tight-binding band-structure calculations were performed on a two-dimensional hexagonal crystal model, using Hamiltonian matrix elements calculated by semiempirical LCAO (linear combination of atomic orbitals) methods. The calculated value for the band gap of hexagonal BN was in reasonably good agreement with the experimental value obtained in the present work, as well as with values reported earlier from electron-energy-loss and photoelectron-emission measurements. The calculations also predicted a very small change in the band gap with temperature, in agreement with the experimental observations.

I. INTRODUCTION

Hexagonal boron nitride is very similar to graphite. The band structure of graphite has been investigated extensively, and a great deal of theoretical work (mostly recent) has also been done on hexagonal boron nitride.[1–5] Still, the calculated theoretical values for the direct optical band gap E_g in hexagonal boron nitride are quite scattered and range between $E_g = 2.45$ eV (Ref. 4) and 5.4 eV (Ref. 2).

Many workers have attempted to determine E_g experimentally. The experimental methods used were soft-x-ray photoemission,[6] electron spectroscopy,[7] electron energy loss,[8] optical reflection,[9,10] and optical absorption in thin films.[11–14] The experimental values found for E_g range between 3.6 eV (Ref. 6) and 5.9 eV (Ref. 13).

From reflectance measurements on hexagonal-boron-nitride powders, Larach and Shrader[9] concluded that $E_g > 5.5$, and Choyke[10] found that reflectivity increases at energies higher than 4.1 eV. The latter also observed another prominent peak at 6.2 eV.

Determination of E_g by optical-absorption measurements of hexagonal-boron-nitride films was carried out by Rand and Roberts[11] who gave the value $E_g = 3.8$ eV, by Noreika and Francombe[12] who obtained $E_g = 4.9–5.2$ eV, by Baronian[13] who obtained $E_g = 5.9$ eV, and by Zupan and Kolar[14] who gave the value $E_g = 4.3$ eV. It should be noted that all the absorption measurements, except those by Baronian, were taken on comparatively thick films (>6000 Å), which limited the range of the measurements to energies below 5.5 eV.

In the present work we report results of optical measurements of hexagonal BN in the range 3.9–6.4 eV, and give band-structure calculations on the same crystal. The experimental values are shown to agree well with the calculated ones.

II. EXPERIMENTAL RESULTS

Our measurements were carried out on thin hexagonal BN films grown by Baronian[13] on quartz substrates, using chemical vapor deposition. The films were polycrystalline, with their optical axis perpendicular to the substrate. We report here results obtained on a film of thickness $d = 680 \pm 50$ Å, as determined interferometrically.

Optical-absorption measurements were carried out with a Cary 14-R spectrophotometer. The samples were mounted in an optical cryostat provided with a heater, which permitted measurements at various temperatures in the range 4.2–700 °K. Reflection measurements were carried out at normal incidence and room temperature, in a system constructed by Naveh.[15]

Photoconductivity measurements were also performed on the same film, using two evaporated aluminum electrodes. The space between the electrodes was illuminated with monochromatic light obtained from a stabilized high-pressure xenon lamp in conjunction with a Hilger D-285 monochromator. The observed photocurrent was very weak, even with widely opened monochromator slits, which decreased the accuracy of the mea-

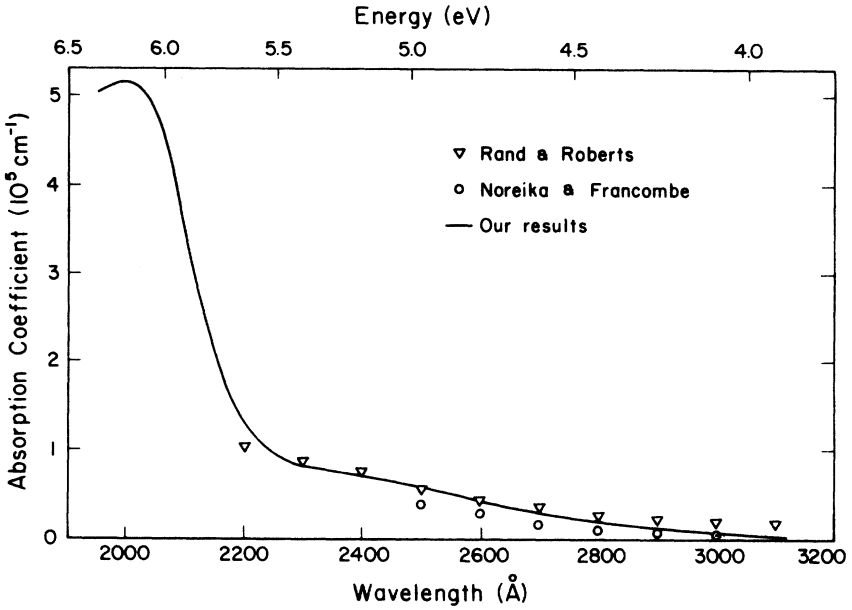

FIG. 1. Absorption coefficient of the BN film at room temperature.

surements.

Figure 1 shows the absorption coefficient K of the hexagonal BN film at room temperature, in the range 1950–3200 Å (6.36–3.87 eV). The absorption coefficient was obtained from the approximate formula $T = \exp(-Kd)$, where T is the transmittance and d is the film thickness. T was determined by comparing the intensity of the light which emerged through the sample, with that passing through the substrate alone. Absorption coefficients computed from the experimental data given by Rand and Roberts,[11] and by Noreika and Francombe[12] are also given in Fig. 1, for comparison. Figure 2 shows the absorption of the hexagonal BN sample

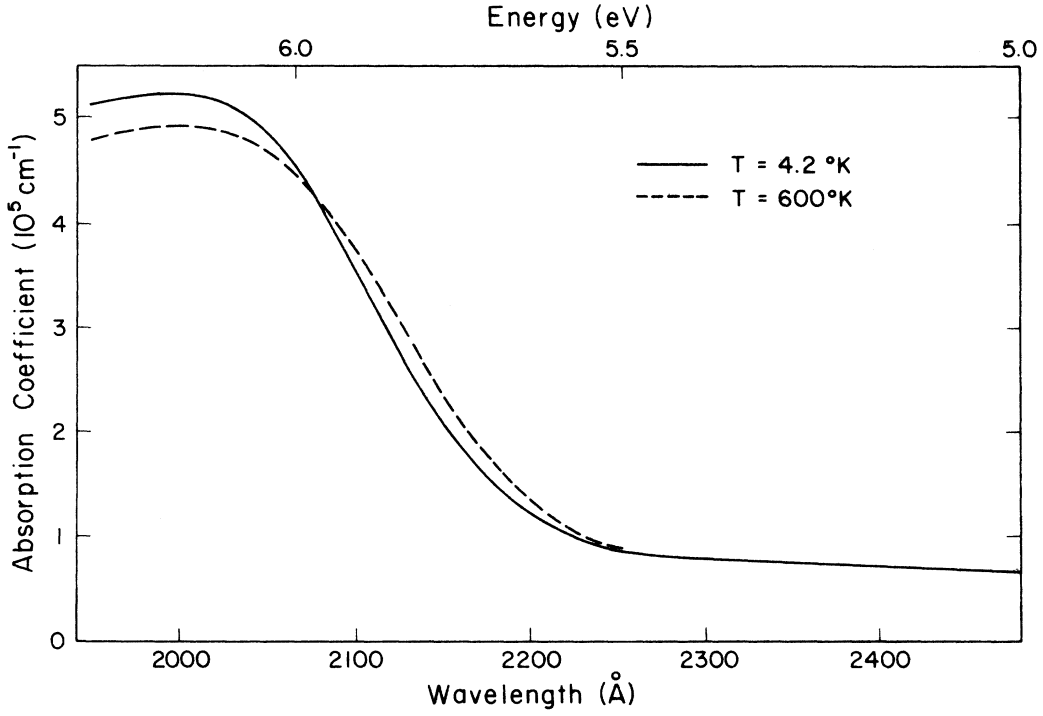

FIG. 2. Absorption coefficient of the BN film at 4.2 and 600 °K.

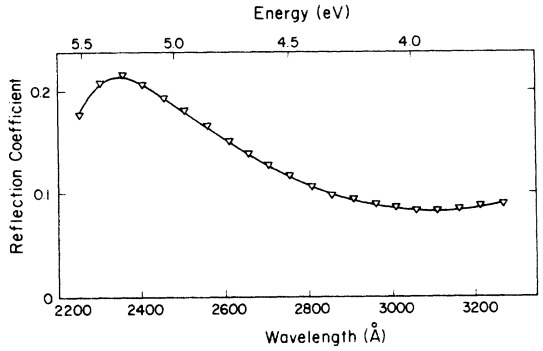

FIG. 3. Reflectance factor of thin BN film at room temperature.

at liquid-helium temperature and at 600 °K. If there is a shift of the high-temperature spectrum to longer wavelengths, it is less than 10 Å (or less than 4×10^{-5} eV/ °K) being an order of magnitude smaller than the corresponding shift in cubic III-V compounds.[16]

Figure 3 shows the reflection factor R of the sample[17,18] as measured at room temperature. A peak near 2300 Å is indicated. This was the short-wavelength limit of our reflection measurements setup, and its accuracy is therefore lower than that of the corresponding high-wavelength data.

Figure 4 shows the photocurrent excitation spectrum of the hexagonal BN sample at room temperature, and also that of a pyrolitic BN (PBN) sample. The spectra were corrected for the intensity distribution of the exciting light. Both spectra are practically the same, showing quite a sharp peak at about 2300 Å. The dependence of the photocurrent on light intensity was almost linear throughout a wide range of intensities. The photocurrent was found to increase gradually with temperature over the whole range of our measurements (100–400 °K).

III. BAND-STRUCTURE CALCULATIONS

The band structure is calculated here by a self-consistent modification of the tight-binding approximation. Previous calculations on hexagonal BN were performed by Nakhmanson and Smirnov[4] by the orthogonal-plane-wave (OPW) method, by Doni and Parravicini[2] who used the experimentally adjusted tight-binding method, and by Zupan[3] and Zunger[5] who applied various semiempirical molecular-orbital (MO) methods to the tight-binding scheme.

Bloch functions $\Phi_\mu^\alpha(\vec{K},\vec{r})$ centered on crystal sublattice sites $\alpha=1,2\ldots h$ and composed of atomic orbitals $\mu=1,2\ldots\sigma$ are defined by:

$$\Phi_\mu^\alpha(\vec{K},\vec{r})=N^{-1/2}\sum_n e^{i\vec{K}\cdot\vec{R}_n}\chi_\mu^\alpha(\vec{r}-\vec{R}_n)\ , \tag{1}$$

where $\chi_\mu^\alpha(\vec{r}-\vec{R}_n)$ is an atomic orbital with $\mu=2s$, $2p_x$, $2p_y$, $2p_z$ centered on site α at unit cell n and $N^{-1/2}$ is the normalization factor. The crystal eigenfunctions $\psi_j(\vec{K},\vec{r})$ are generated by forming linear combinations of these $h\sigma$ Bloch functions. The combinations coefficients $C_{\mu j}^\alpha(\vec{K})$ are solutions of the secular equations:

$$\sum_{\mu=1}^{\sigma}\sum_{\alpha=1}^{h}[F_{\mu\nu}^{\alpha\beta}(\vec{K})-S_{\mu\nu}^{\alpha\beta}(\vec{K})\,\delta_j(\vec{K})]\,C_{\mu j}^\alpha(\vec{K})=0\ , \tag{2}$$

where the matrix elements between the Bloch functions are given by

$$\begin{aligned}F_{\mu\nu}^{\alpha\beta}(\vec{K})&=\sum_n e^{i\vec{K}\cdot(\vec{R}_n-\vec{R}_0)}\langle\chi_\mu^\alpha(\vec{r}-\vec{R}_0)\,|\,\hat{F}\,|\,\chi_\nu^\beta(\vec{r}-\vec{R}_n)\rangle\\&\equiv\sum_m e^{i\vec{K}\cdot\vec{R}_m}H_{\mu\nu}^{\alpha\beta}(0-m)\ ,\\S_{\mu\nu}^{\alpha\beta}(\vec{K})&=\sum_n e^{i\vec{K}\cdot(\vec{R}_n-\vec{R}_0)}\langle\chi_\mu^\alpha(\vec{r}-\vec{R}_0)\,|\,\chi_\nu^\beta(\vec{r}-\vec{R}_n)\rangle\\&\equiv\sum_m e^{i\vec{K}\cdot\vec{R}_m}S_{\mu\nu}^{\alpha\beta}(0-m)\ .\end{aligned} \tag{3}$$

The origin unit cell is chosen at $\vec{R}_0$ and $\hat{F}$ denotes the Hartree–Fock energy operator. The matrix elements $H_{\mu\nu}^{\alpha\beta}(0-m)$ [Eq. (3)] can be calculated either in the conventional tight-binding scheme or in the self-consistent approach. In the former case, fixed free-atom (or free-ion) potentials are used to generate the crystalline potential and thus the $H_{\mu\nu}^{\alpha\beta}(0-m)$ elements do not depend on the complete set of the occupied band eigenvectors, but rather on the pair of basis orbitals χ_μ and χ_ν. In the self-consistent scheme,

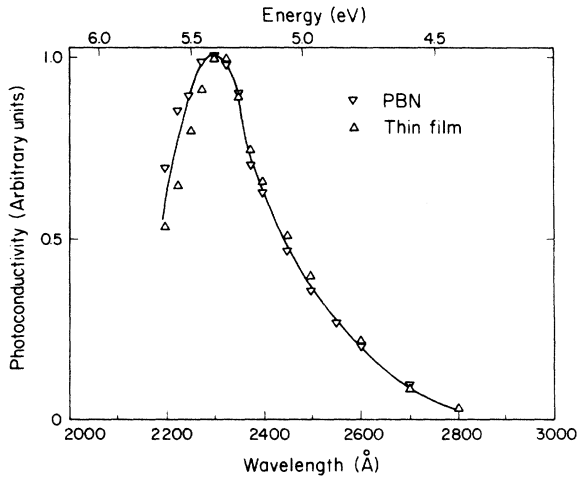

FIG. 4. Excitation spectrum of the photoconductivity of pyrolitic BN (PBN) and a thin film of BN at room temperature.

on the other hand, charge redistribution effects are considered, and the free-atom potentials are allowed to modify in the crystalline environment either by introduction of screening or by re-evaluating them at each iteration cycle on the basis of the calculated valence charge density. The elements of the valence-charge-density matrix are defined in terms of the expansion coefficients $\{C^{\alpha}_{\mu j}(\vec{K})\}$ of all $(\sigma h)_{oc}$ occupied bands by

$$P^{\alpha\delta}_{\mu\nu}(n-m) = \frac{1}{\Omega}\int_{BZ} d\vec{K} \sum_{j=1}^{(\sigma h)_{oc}} n_j C^{\alpha *}_{\mu j}(\vec{K})\, \delta^{\sigma}_{\nu j}(\vec{K}) \times e^{i\vec{K}\cdot(\vec{R}_n-\vec{R}_m)}\, \chi^{\alpha}_{\mu}(\vec{r}-\vec{R}_0)\, \chi^{\delta}_{\nu}(\vec{r}-\vec{R}_m)\ , \quad (4)$$

where Ω is the volume of the occupied part of the Brillouin zone (BZ) and n_j is the occupation number. Equivalently, when a direct linear combination of atomic orbitals (LCAO) expansion of $\Psi_i(\vec{r})$ in terms of the N crystal orbitals

$$\Psi_i(\vec{r}) = T^{-1} \sum_{n=1}^{N} \sum_{\mu=1}^{\sigma} \sum_{\alpha=1}^{h} D^{n\alpha}_{\mu i}\, \chi^{\alpha}_{\mu}(\vec{r}-\vec{R}_n)\ ; \quad i = 1 \ldots \sigma h N\ , \quad (5)$$

is employed, the BZ integration is replaced by a direct sum, yielding

$$P^{\alpha\delta}_{\mu\nu}(n-m) = N^{-1} \sum_{i=1}^{N_{oc}} n_i\, D^{n\alpha}_{\mu i}\, D^{m\delta}_{\nu i}\, \chi^{\alpha}_{\mu}(\vec{r}-\vec{R}_n)\chi^{\delta}_{\nu}(\vec{r}-\vec{R}_m). \quad (6)$$

T^{-1} indicates the normalization of the crystal function $\Psi_i(\vec{r})$ Eq. (5) and N_{oc} denotes the number of occupied levels in the crystal. The diagonal $P^{\alpha\alpha}_{\mu\mu}(0)$ element represents the μ-orbital charge on site α due to all occupied levels in the crystal. The net atomic charge is given by

$$Q_{\alpha n} = Z_{\alpha n} - \sum_{\mu=1}^{\sigma} P^{\alpha\alpha}_{\mu\mu}(0)\ , \quad (7)$$

where $Z_{\alpha n}$ is the α-core charge. In self-consistent schemes, the elements $H^{\alpha\delta}_{\mu\nu}(0-m)$ are expressed by the $P^{\alpha\delta}_{\mu\nu}(0-m)$ elements or by the net charges $Q_{\alpha n}$, these quantities being determined by all occupied crystal eigenvectors, while in non-self-consistent treatments, the $Q_{\alpha n}$'s are implicitly assumed to attain their free-atom (or free-ion) values (equal to zero for neutral atoms and to the ionic valency for free ions). In what follows, we will use several of the self-consistent as well as non-self-consistent approximations to the $H^{\alpha\delta}_{\mu\nu}(0-m)$ elements adopted in semiempirical MO calculations in molecules. The band structure of hexagonal boron nitride will be computed using these methods, examining the role of self-consistency. The approximations to be considered are the following.

A. Extended-Hückel (EXH)

In this non-self-consistent approximation,[19] the off-diagonal matrix dements are given by

$$H^{\alpha\delta}_{\mu\nu}(0-m) = \tfrac{1}{2} G\,(H^{\alpha\alpha}_{\mu\mu} + H^{\delta\delta}_{\nu\nu})\, S^{\alpha\delta}_{\mu\nu}(0-m)\ , \quad (8)$$

where the overlap integral $S^{\alpha\delta}_{\mu\nu}(0-m)$ is calculated from Slater-type atomic orbitals χ_μ and χ_ν centered on sites α and δ, respectively, in unit cells located at $\vec{R}_0$ and $\vec{R}_n$, respectively. The diagonal elements $H^{\alpha\alpha}_{\mu\mu}$ represent the valence-state ionization potential of the orbital located at site α and is determined from spectroscopical data,[20] while G is the empirical Wolfsberg-Helmholz constant, taking the value 1.75.[19] The relation of the EXH approximation to the Hartree-Fock scheme has been previously discussed by Blyholder and Coulson,[21] and by Gilbert.[22] The method has been previously used successfully for computing the electronic structure of many organic molecules[19a] as well as boron-nitrogen compounds.[19b]

B. Iterative extended Hückel (IEXH)

In this self-consistent refinement of the simple EXH method, the matrix elements are allowed to modify according to the self-consistent charge in the system under consideration.[23,24] The off-diagonal matrix elements are given by the Cusachs approximation[25] which is second order in the overlap integrals and thus better accounts for the kinetic-energy contribution to the matrix element

$$H^{\alpha\delta}_{\mu\nu}(0-m) = [H^{\alpha\alpha}_{\mu\mu}(Q_{\alpha 0}) + H^{\delta\delta}_{\nu\nu}(Q_{\delta m})] \times \{1 - \tfrac{1}{2}|S^{\alpha\delta}_{\mu\nu}(0-m)|\} S^{\alpha\delta}_{\mu\nu}(0-m)\ . \quad (9)$$

The overlap integrals are calculated from Slater's atomic orbitals as in the EXH method. The diagonal matrix elements are taken to depend explicitly on the charge

$$H^{\alpha\alpha}_{\mu\mu}(Q_{\alpha n}) = H^{\alpha\alpha}_{\mu\mu}(0) + Q_{\alpha n}\Delta^{\mu}_{\alpha n} + \sum_{\beta m \neq \alpha n} Q_{\beta m}\gamma_{\alpha n,\beta m}\ . \quad (10)$$

$H^{\alpha\alpha}_{\mu\mu}(0)$ is the atomic μ-orbital energy of the neutral ($Q_{\alpha n}=0$) atom, determined either from atomic spectroscopy or from Hartree-Fock calculations on neutral atoms.[26] $\Delta^{\mu}_{\alpha n}$ is the change in the μ-orbital energy of atom αn due to the presence of a nonzero charge $Q_{\alpha n}$ on this site. It is evaluated from the interpolation scheme suggested by Cusachs and Reynolds[26] based on spectroscopically measured orbital energies of atoms carrying different charges. In the calculation of the net atomic charges $Q_{\alpha n}$, we adopt the procedure of Rein *et al.*,[23] avoiding the arbitrary partitioning of the heteropolar bond charge into equal parts.[27] The net charges are calculated from both the one-center and the two-center contributions to the charge moment, thus preserving the nonspherical character of the bond. $\gamma_{\alpha n,\beta m}$ denotes the average two-center Coulomb interaction between an orbital on atom αn with that on atom βm and is calculated analytically for Slater orbitals following Ref. 28.

Expression (10) for the diagonal element has a simple physical interpretation. The first term represents the contribution of an isolated neutral atom, the second term corrects for deviation from neutrality at a particular site due to the bonding in the crystal, while the third term represents screened Madelung-type electrostatic forces exerted by the rest of the crystal. In many applications of the iterative extended Hückel method in molecular calculations, only the first two terms in Eq. (10) are retained. In the calculations to be presented we examine both this approach (denoted as simple IEXH or SIEXH) and that based on all terms in Eq. (10) (denoted as (MIEXH).

C. Complete neglect of differential overlap (CNDO)

In this scheme, the matrix elements are given by

$$H^{\alpha\delta}_{\mu\nu}(0-n) = -\beta^0_{\alpha\delta} S^{\alpha\delta}_{\mu\nu}(0-n) - \tfrac{1}{2} P^{\alpha\delta}_{\mu\nu}(0-n)\gamma_{\alpha 0,\delta n}\,, \tag{11}$$

$$H^{\alpha\alpha}_{\mu\mu} = -\tfrac{1}{2}(I_\alpha + A_\alpha) - \{Q_{\alpha 0} + \tfrac{1}{2}[P^{\alpha\alpha}_{\mu\mu}(0) - 1]\}\gamma_{\alpha 0,\alpha 0} + \sum_{\delta n \neq \alpha 0} Q_{\delta n}\gamma_{\delta n,\alpha 0}\,, \tag{12}$$

where $\beta^0_{\alpha\delta}$ is the bonding parameter, $P^{\alpha\delta}_{\mu\nu}(0-n)$ represents the $(\mu\alpha)-(\nu\delta)$ elements of the bond order and charge matrix in the zero-overlap approximation. $\gamma_{\delta n,\alpha 0}$ are the two-center integrals evaluated in the Mataga approximation,[29] $-\frac{1}{2}(I_\alpha + A_\alpha)$ are the Mulliken-type[28] atomic electronegativities, and $Q_{\alpha 0}$ is the net electronic charge on atom α.

In view of the substantial electronegativity difference between the atoms constituting the primitive cell of boron nitride (electronegativities on the Pauling's scale: boron 2.0 and nitrogen 3.0) one would expect significant charge redistribution to occur in the crystal. Self-consistent[30] APW (augmented plane wave) and [31]OPW calculations on other binary solids, have indicated that self-consistency is indeed essential for obtaining a reliable band structure. Non-self-consistent tight-binding calculations previously performed on boron nitride[2] yielded poor agreement with optical data unless the various matrix elements involved were scaled to yield a better fit. A self-consistent tight-binding calculation [Eqs. (1)–(7)] on the other hand, necessitates the somewhat involved computation of the charge-density matrix through numerical integration Eq. (4) in the Brillouin zone.[32,33] This procedure will be used here for computing the band structure of hexagonal boron nitride, when the BZ integration in Eq. (4) is replaced by a sum over 180 $\vec{K}$ points in the $\frac{1}{12}$ irreducible section of the BZ. The results of this calculation will be compared with those yielded by the cluster band-structure calculation. The latter approach is based on the observation that in covalent structures, the $H^{\alpha\delta}_{\mu\nu}(0-n)$ elements are mainly affected by the charge distribution of a relatively small number of atoms surrounding the $0-n$ bond. Thus, one might hope to approximate the self-consistent limit of these elements by evaluating them from a self-consistent LCAO calculation of a finite cluster of atoms that are arranged geometrically according to the known crystal packing. The cluster's wave function assumes the form given in Eq. (5), and the charge matrix elements are computed in direct space in Eq. (6). The dependence of the $H^{\alpha\delta}_{\mu\nu}(0-n)$ elements on the size of the cluster should then be examined by increasing the cluster size and seeking the convergence limit of the elements where the $\vec{R}_0$ position is taken at the center of the cluster and the distance $|\vec{R}_n - \vec{R}_0|$ is limited to be much smaller than the cluster's radius. In predominantly covalent structures, where the chemical bonding is determined by the charge distribution in the vicinity of the bonds, this procedure should rapidly converge yielding thereby the self-consistent value of the interaction matrix elements. These are then used to compute the band structure throughout the BZ using Eqs. (1)–(3). Such an approach is attractive because it supplies a means of correlating the electronic structure of isolated molecular fragments with related solids. It was previously adopted by Coulson *et al.*[34,35] in calculating the π band structure of graphite and boron nitride by employing matrix elements obtained from calculations on benzene and borazine molecules, respectively. A similar idea was recently adopted by Zupan[3] for hexagonal boron nitride in which the atomic potentials of boron and nitrogen atoms needed for solving Eq. (2), were transferred from the separate CNDO calculation on the N_3B and B_3N clusters, respectively. To approximately preserve the correct hybridization of the central atom in these clusters, one is forced to artificially reduce the number of electrons of the "ligand" atoms to one-third, generating thereby for the central atom, a different electronic environment than it would have in the crystal. Also, due to the presence of three "dangling" bonds on the edges of these clusters, the potential at their center may exhibit severe distortions (see below).

A more general approach used here employs finite molecular clusters to obtain self-consistent matrix elements for band-structure calculations. We first solve for the eigenvalues of a sequence of finite boron-nitridelike clusters of gradually increasing size (Fig. 5) using the SIEXH and CNDO methods. We seek the convergence limit of the various matrix elements $H^{\alpha\delta}_{\mu\nu}(0-n)$, relating pairs of atoms up to second neighbors ($n=0, 1, 2$), where the atom situated at $\vec{R}_0$ is chosen as the innermost atom of each cluster (see Fig. 5) and the elements are taken from the last self-consistent iteration.

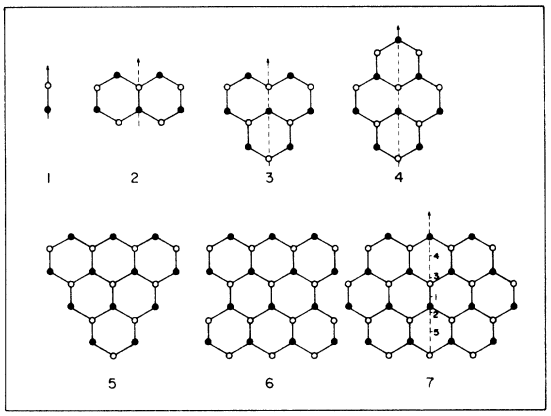

FIG. 5. Molecular hexagonal BN clusters. Open and dark circles denote different types of atoms. The vertical arrows on clusters 1, 2, 3, 4, and 7 denote the direction in which electrostatic potentials are computed (Table I and Fig. 6). The four central atoms that are considered for matrix elements calculations are joined by heavy lines (clusters 5–7). R_{BN} was taken as 1.446 Å. The numbering in cluster 7 (see Table I) denote selected points for computing comparative potentials. Taking point 1 as the origin ($R_1=0$) the distances are: $R_2=-(\frac{1}{2}+\delta)R_{BN}=-0.733$ Å, $R_3=(\frac{1}{2}+\delta)R_{BN}=0.733$ Å, $R_4=\frac{5}{3}R_{BN}=2.410$ Å, $R_5=-\frac{3}{2}R_{BN}=-2.169$ Å, where δ was taken as 0.01 Å.

The geometry of these finite clusters is chosen to simulate the experimentally known hexagonal-boron-nitride structure with $R_{BN}=1.446$ Å.[36] Hydrogen atoms attached to each atom on the edges of the cluster (with boron-hydrogen distance $R_{BH}=1.2$ Å and nitrogen-hydrogen distance $R_{NH}=1.1$ Å) to saturate the "free valences" of the otherwise dangling bonds. Addition of hydrogen atoms to the cluster's surface, has been shown[5] to suppress efficiently the charge inhomogeneity on the various sublattices in the cluster model.

In order to estimate the largest $0-n$ distance within which the perturbations exerted by the cluster's surface do not penetrate, we use the electrostatic Poisson potential obtained from the cluster's wave functions as a monitor. We thus solve for the electronic Poisson potential $V_{elec}(\vec{r}-\vec{R})$ from

$$\nabla^2 V_{elec}(\vec{r}-\vec{R})=4\pi\rho(\vec{r}-\vec{R}) , \tag{13}$$

where $\rho(\vec{r}-\vec{R})$ is the electron density distribution obtained from the wave functions $\Psi_i(\vec{r})$ (directly calculated from the solution of the clusters LCAO equations)

$$\rho(\vec{r}_1-\vec{R})=\sum_{i=1}^{N_{OC}}\psi_i^*(\vec{r}_1,\vec{r}_2,\ldots,\vec{r}_N)\times\psi_i(\vec{r}_1,\vec{r}_2,\ldots,\vec{r}_N)\,d\tau_2\cdots d\tau_N . \tag{14}$$

The total electrostatic potential is obtained as a sum of $V_{elec}(\vec{r}-\vec{R})$ from Eq. (13) and the nuclear potentials

$$V(\vec{r}_i-\vec{R})=-V_{elec}(\vec{r}_i-\vec{R})+\sum_{\alpha,n}\frac{Z_{\alpha n}}{|\vec{R}_n-\vec{r}_i+\vec{d}_\alpha|} , \tag{15}$$

where d_α is the position vector of site α in the unit cell.

In recent works[37] it has been demonstrated that the CNDO wave function reproduces quite accurately the electrostatic potential as calculated by *ab initio* wave functions for small and medium size molecules. The Poisson potential $V(\vec{r}-\vec{R})$ generated by all occupied MO's, can be analytically computed[38] when the atomic basis set employed in the SCF-MO (self-consistent-field molecular orbitals) calculation is represented by Gaussians. Since we use a Slater rather than a Gaussian basis set, we expand each Slater orbital in a series of Gaussians using the $6-G$ expansion of Hehre.[39]

IV. RESULTS AND DISCUSSION

A. Crystalline band structures

The band structure of the two-dimensional boron nitride along the $P-\Gamma-Q-P$ direction (notation of Ref. 2) as calculated by the various approximations to the tight-binding matrix elements, is revealed in Fig. 6. Three orders of neighbors were retained in the calculation of overlap-depended matrix elements, while the screened electrostatic terms were summed within a constant radius of 65 Å. In the case of self-consistent computation, 180 inequivalent $\vec{K}$ points in the $\frac{1}{12}$ irreducible part of BZ were employed for the integration of the density matrix. The iteration cycle is terminated when the charges and one-electron energies in successive iterations agree within $10^{-2}e$ and 10^{-3} a.u., respectively. Interband transitions at some high-symmetry points are given in Table I and compared with the available experimental data. The present optical study indicates that the band gap occurs at 5.8 eV and an intense peak is observed at about 6.2 eV. These are assigned to the direct $\pi\rightarrow\pi^*$ gap at $P_1^-\rightarrow P_2^-$ and to the saddle-point transition $Q_2^-\rightarrow Q_2^-$, respectively. Both the noniterative EXH calculation and the fully self-consistent MIEXH calculation retaining all terms in the Hamiltonian, yield very close results and agree quite favorably with the experimental data, while the simple iterative scheme retaining only the first two terms in the Hamiltonian (SIEXH) significantly underestimates the band gap at $P_1^-\rightarrow P_2^-$ and yields lower values for the other transitions given in Table I. The latter calculation also does not reveal any $\sigma-\pi$ overlap at the zone center ($\Gamma_3^+-\Gamma_2^-$) due to an upward shift of the valence π band and a downward shift of the conduction π^* band. The existence of such a $\sigma-\pi$ overlap has been previously established in the related systems of graphite[41–43]

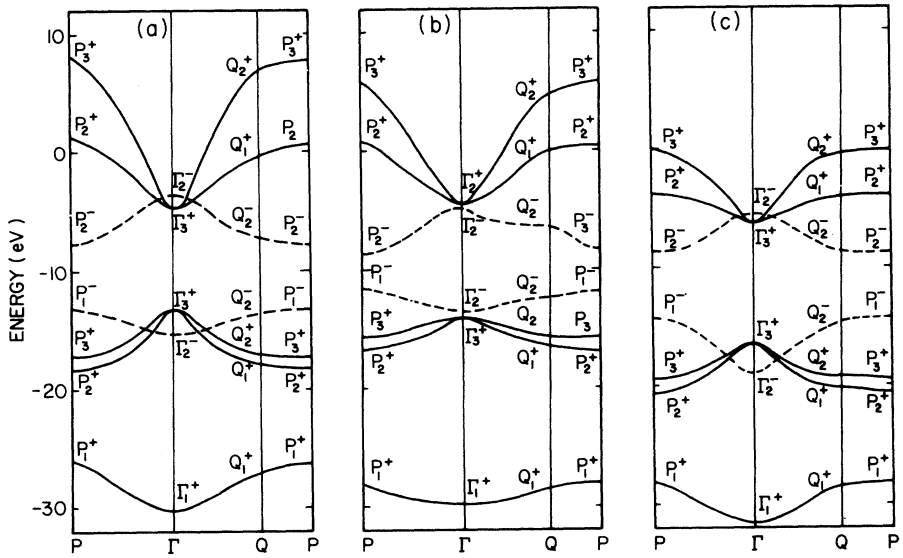

FIG. 6. Band structure of two-dimensional hexagonal boron nitride. Dashed lines indicate π bands. The highest occupied valence state is P_1. (a) Extended Huckel (EXH); (b) simple iterative extended Hückel (SIEXH); (c) modified iterated extended Hückel (MIEXH).

and borazine[44,45] (1.2 eV) and seems to be consistent with the interpretation of the x-ray photoemission data of hexagonal boron nitride.[46]

An examination of the various terms appearing in the Hamiltonian elements [Eq. (5)] reveals the reason for the contrasting behavior of SIEXH compared with both EXH and MIEXH results. The simple iterative scheme (SIEXH) tends to lower the atomic orbital energies of the positively charged boron sublattice, and to increase the atomic orbital energies of the negatively charged nitrogen sublattice [Eq. (5)]. These changes, associated with the one-center terms are very sensitive to the charge redistribution relative to the neutral atoms, due to the substantial magnitude of the $\Delta^{\mu}_{\alpha n}$ terms, the latter being of the same order as the zero-order $H^{\alpha\alpha}_{\mu\mu}(0)$ terms.[26] In the absence of the electron repulsion effects due to other centers, the one-center terms tend to neutralize the strong charge build-up characterizing the noniterative scheme ($Q_B = -Q_N = 1.27e$ in EXH) resulting in low ionicities ($Q_B = -Q_N = 0.30\ e$ in SIEXH) and a decreased band gap ($E_g = 3.7$ eV). The lowering in the boron orbital energy and the increase in the nitrogen orbital

TABLE I. Interband transition energies in hexagonal boron nitride, calculated from the crystal band structure, as compared with experimental data. All values given in eV.

	Crystal band structure				Experimental data	
Transition	EXH	SIEXH	MIEXH	Optical data (Present work)	Electron energy loss	Photoelectrons
$P_1^- \rightarrow P_2^-$ ($\pi \rightarrow \pi^*$)	5.5	3.7	5.1	5.8		4.4,[a] 3.6[b]
$Q_2^- \rightarrow Q_2^-$ ($\pi \rightarrow \pi^*$)	6.3	6.0	6.3	6.2	6.5,[c] 6.3,[d] 6.2[e]	
$Q_2^+ \rightarrow Q_2^-$ ($\sigma \rightarrow \pi^*$)	9.4	8.9	9.3		9.4[c]	
$\Gamma_3^+ \rightarrow \Gamma_3^+$ ($\sigma \rightarrow \sigma^*$)	8.2	9.2	10.4		10.4[d]	
$Q_2^+ \rightarrow Q_1^+$ ($\sigma \rightarrow \sigma^*$)	15.0	14.1	14.9		14.1[c]	

[a]K. Hamrin *et al.* Ref. 7.
[b]V. A. Formichev, Ref. 6.
[c]R. Vilanove, Ref. 8.
[d]M.J. Cazaux, Ref. 40.
[e]W.J. Choyke, Ref. 10.

energy due to the linear one-center terms is most pronouncedly revealed by the decrease in the band gap between the zone corner P_1^- and P_2^- states that are pure nitrogen and boron $2p_z$ Bloch states, respectively, while the zone center (Γ) and zone-edge (Q) points are affected to a smaller extent due to interference of boron and nitrogen Bloch functions at these points in the BZ (compare Figs. 6(a) and 6(b). This leads to an increased dispersion of the π bands, a $\sigma-\pi$ separation and, an increase in the π valence-band width and to a decrease in the ionization potential ($=-\mathcal{E}_{P_1^-}$) in the SIEXH results relative to the EXH results. When the two-center electrostatic terms are included in the Hamiltonian elements (MIEXH), they tend to cancel the one-center terms due to the alternating signs of the charges on the two sublattices. The electrostatic terms thus screen effectively the one-center terms, resulting in a much lower dependence of the atomic orbital energies on charges (and hence the iteration procedure converges more rapidly) and in a reduction in the degree of charge neutralization characterizing the SIEXH scheme. The noniterative EXH method thus becomes a good approximation to the complete self-consistent MIEXH method regarding one-electron energies, whereas the latter method is still better for charges ($Q_B=-Q_N=0.55\ e$ in MIEXH). The inclusion of the Madelung-type terms results in an over-all stabilization of the bands. Owing to the larger stabilization of the bonding valence bands, the onset of $\sigma\rightarrow\sigma^*$ transition ($\Gamma_3^+\rightarrow\Gamma_3^+$) increases to 10.4 eV and a smaller increase occurs in the saddle-point transitions at Q (see Table I). The $\sigma-\pi$ overlap at the valence-band zone center increases to 2.2 eV and the π band width to 5.1 eV. This behavior of the Madelung-type terms is consistent with the apparent success of the simple EXH method and explains the abnormally low-energy gap previously obtained in SIEXH calculations.[47] Similar near-cancellation effects between Madelung and linear terms in the charge have been previously observed in heteropolar molecules.[48,49] Inclusion of spherical Madelung terms has been shown to increase the ionicities and the energy of the lowest transition, and to reduce drastically the charge dependence of the orbital energies.[48,49] Further examination of matrix-elements effects on the calculated optical spectra of boron nitride, using our band structure, would help to assess these results.

It is interesting to compare the characteristics of the band gap in the hexagonal and the cubic modifications of boron nitride in view of the various terms determined the diagonal and nondiagonal matrix elements. The lowest band gap in *cubic boron nitride* is indirect and involves the energy difference between the conduction X_1 state and the zone center valence Γ_{15} state.[50,51] The irreducible representations of the cubic space group at these points[50] allow mixing of the Bloch functions belonging to the boron and nitrogen sublattices both at Γ_{15} and at X_1 and consequently the band gap E_g involves both a heteropolar E_{gc} term proportional in the first neighbor approximation to the differences in orbital energies of the two atoms in the unit cell:

$$E_{gc}\propto H^{B,B}_{2p,2p}(Q_B)-H^{N,N}_{2p,2p}(Q_N)$$
$$=\left(H^{B,B}_{2p,2p}(0)+Q_a\Delta^{2p}_B+\frac{MQ_a}{R_{BN}}\right)$$
$$-\left(H^{N,N}_{2p,2p}(0)-Q_a\Delta^{2p}_N-\frac{MQ_a}{R_{BN}}\right)\quad,\tag{16}$$

and a homomolar E_{gh} term, proportional to the interaction element between the two sublattices

$$E_{gh}\propto H^{B,N}_{2p,2p}(R_{BN})\ .\tag{17}$$

In these expressions Q_a denotes the positive net charge of the $B^{+Q_a}N^{-Q_a}$ system and MQ_a/R_{BN} represents the classical Madelung term. In *hexagonal boron nitride*, the direct gap involves the P_1^- and P_2^- states. The irreducible representations of the hexagonal group at these points does not allow any mixing between the Bloch states belonging to the different sublattices[2] and consequently, the band gap in the hexagonal form is purely heteropolar [Eq. (16)]. Thus, in terms of the dispersion dielectric theory of Phillips and Van Vechten,[52] cubic boron nitride exhibits an average homopolar-heteropolar gap $E_g^{cubic}=(E_{gc}^2+E_{gh}^2)^{1/2}$ while hexagonal boron nitride exhibits a purely heteropolar gap $E_g^{hex}=E_{gc}$.

In the homopolar analogous of boron nitride, namely diamond and graphite, the E_{gc} terms vanishes by symmetry due to the chemical equivalence of the two sublattices. Thus in the hexagonal graphite $E_g=0$, since mixed E_{gh} terms are not involved in the energies of the zone-corner states, while in diamond, the zone-center direct gap is $E_g=E_{gh}$.

It has been pointed out by Phillips[53] that the $Q_a=0$ approximation for the heteropolar band gap in diamondlike binary crystals grossly overestimates the true value, while inclusion of the linear $Q_a\Delta$ terms alone, yields a largely underestimated value due to the absence of a sufficiently large covalent term to oppose the charge redistribution. This difficulty is not present in the dielectric-dispersion model[52,53] since the use of the Penn model with empirical static dielectric constants, automatically accounts for the correct magnitude of the gap. It is shown here, that inclusion of the Madelung-type terms in the self-consistent LCAO scheme, provides for the correct forces opposing the neutralization effects (introduced by the linear

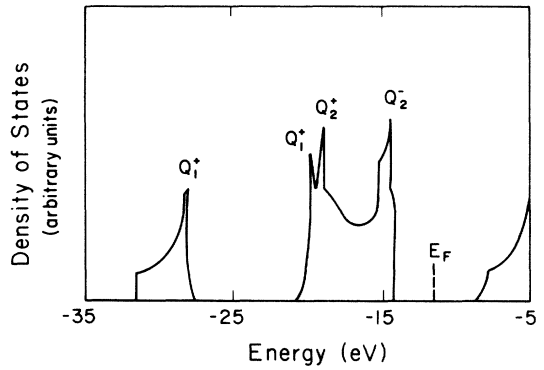

FIG. 7. Density of states in two dimensional hexagonal boron nitride, computed from the MIEXH self-consistent band structure.

$Q_a\Delta$ terms), yielding thereby a proper value for the gap and reasonable charges.

The particular form of the $P_1^- \rightarrow P_2^-$ band gap in hexagonal boron nitride given by Eq. (16) has an interesting implication on the temperature dependence of the gap. Assuming that the major contribution to this dependence results from the temperature effect on the lattice constant, one would predict a very small temperature coefficient to the gap, resulting from the small indirect contribution of the lattice constant to the ionicity Q_a through crystal-field screening effects. The interband transitions at the Γ and Q points, on the other hand, involving homopolar E_{gh} terms that are proportional to the interaction matrix element between neighboring boron and nitrogen atoms, will reveal a much stronger temperature dependence since the nondiagonal $H_{2p,2p}^{B,N}(R_{BN})$ terms are governed by overlap-depending short-range interactions. To test these model conclusions, we have computed the band structure of hexagonal boron nitride for a range of R_{BN} distances corresponding to the experimental bond lengths in the temperature range of 0–700 °C, employing the known thermal expansion coefficient in the layer plane.[36] Fitting the results to a simple relation $E_g = E_g(0) - \beta T$ we obtained $\beta = 1.17\times10^{-5}$ eV/°K by the CNDO method, $\beta = 1.0\times10^{-5}$ eV/°K by the SIEXH method, and $\beta = 9\times10^{-6}$ eV/°K by the MIEXH method. These compare reasonably with the experimental upper bound of $\beta \leq 4\times10^{-5}$ eV/°K. In the non-self-consistent EXH calculation, the diagonal $[H_{2p,2p}^{B,B}(0) - H_{2p,2p}^{N,N}(0)]$ term does depend on distance and hence a zero-temperature coefficient is revealed. When additional neighbors are included in Eq. (16), the gap is shown to depend on $[H_{2p,2p}^{B,B}(2) - H_{2p,2p}^{N,N}(2)]$, i.e., on the second-nearest-neighbor B-B and N-N pairs. This contributes a small part to β and indeed the EXH band calculation yields a small value of $\beta = 7.8\times10^{-6}$ eV/°K. The saddle-point $\pi \rightarrow \pi^*$ transition at Q_2^- reveals a much higher temperature coefficient: $\beta = 2.1 \times10^{-3}$ eV/°K (MIEXH result), which is of the order of magnitude observed in zone-center transitions in binary diamond and Wurzite crystals.[54]

The density of valence states in hexagonal boron nitride (Fig. 7) was calculated from the MIEXH band structure using 9800 $\vec{K}$ points interpolated by the Lagrange formula from 180 directly calculated $\vec{K}$ points in the irreducible section of the BZ. The peaks in the density of states are assigned to the saddle-point singularities at the Q points. Photoelectron spectroscopy[7] in hexagonal boron nitride reveals four peaks in the valence band, with binding energies (in eV) relative to the Fermi level E_F of $19.4+E_F$, $11.4+E_F$, $9.0+E_F$, and $3.9+E_F$. If the Fermi level is assigned to the center of the forbidden gap, the four calculated singularities (MIEXH results) occur at $19.5+E_F$, $8.8+E_F$, $7.8+E_F$, and $3.4+E_F$, respectively. These agree favorably with the experimental data. The interpretation of the x-ray spectra of boron and nitrogen in boron nitride[46] suggested that the Fermi energy is slightly shifted from the center of the gap towards the conduction band. Such a shift would improve the agreement between the calculated and observed photoelectron transitions. Since the work function of boron nitride is not known accurately, it is not possible to determine absolute ionization energies from the experimental binding energies.

The results of the present calculation agree favorably with the result of Doni and Parravicini[2] using an empirical non-self-consistent tight-binding scheme. The latter authors obtained a gap of 5.4 eV, a $\pi \rightarrow \pi^*$ transition energy of 6.6 eV and a valence-band minimum at $16.2+E_F$ ($2S_N$ band minimum). Although the over-all shape of the bands are similar in both calculations, Doni and Parravicini obtained zero overlap between the σ and π bands at the $\Gamma_2^- - \Gamma_3^+$ points and their bands are narrower than ours (π width -1.2 eV, total valence width -13.6 eV compared with 5.1 and 17.3 eV, respectively, in the present calculation). The non-self-consistent OPW calculation of Nakhmanson and Smirov[4] yields a small band gap of 3.6 eV and a very large valence-band width of 27.8 eV. X-ray spectra of boron nitride[6] indicate a total valence-band width of about 18.6 eV.

B. Cluster band structure

In this section we discuss the band structure of hexagonal boron nitride in which the elements $H_{\mu\nu}^{\alpha\beta}(0-n)$ [Eq. (3)] are computed from finite clusters (Fig. 5). We employ both the SIEXH and the CNDO approximations to the matrix elements to facilitate comparison with previous cluster calculations based on these approximations.[3,55]

To verify the adequacy of finite molecular clusters

TABLE II. Net atomic charge of the central nitrogen atom in each of the clusters (Fig. 5) as computed from Mulliken population analysis of CNDO wave functions.

	Cluster 1	Cluster 2	Cluster 3	Cluster 4	Cluster 5	Cluster 6	Cluster 7
Nitrogen atomic charge (e)	−0.1620	−0.1839	−0.1995	−0.2539	−0.2964	−0.3065	−0.3080

to the calculation of matrix elements to be used as input to the band-structure calculation of the infinite solid, we first examine the convergence of atomic charges and electrostatic potentials at the center of the cluster as a function of the cluster's size. Table II shows the net atomic charge Q_N on the central nitrogen atom as computed from the Mulliken population analysis[27] of the CNDO wave function of clusters 1–7 (Fig. 5). It is seen that for clusters as big as cluster 5 or 6 the charge of the central atom is stabilized, indicating that for these clusters the perturbations associated with the dangling bonds at the surface, have little effect on the center. A similar behavior is manifested by the electrostatic Poisson potentials of the finite clusters. Table III shows the total electrostatic potential calculated at selected points (Fig. 5) along the central B-N bond of clusters of increasing size. The potentials near the nuclei (points 2 and 3) converge rapidly as a function of cluster size due to the "hard core" behavior in this region. At the center of the B-N bond (point 1) as well as in the extra-bond region (points 4 and 5) the convergence is slower. A cluster at least as large as cluster 4 should be employed for reliable calculation. The relatively satisfactory convergence of the electrostatic potentials in clusters of typical size denoted in Fig. 5, makes it feasible to obtain the convergence-limit values using a moderate computing time.

It has been previously suggested[3] that small clusters as B_3N and N_3B could be used to approximate the self-consistent matrix elements needed in the band-structure calculations of the infinite solid. We have computed the Poisson electrostatic potential across these clusters, using the corresponding charge densities [Eq. (14)] and compared them with the potential along the B-N bond of the largest cluster considered in the present work (cluster 7, Fig. 5). The results (Fig. 8) indicate that both the B_3N and the N_3B clusters reveal a drastically distorted potential, relative to our convergence limit results, suggesting that the incomplete charge redistribution in small clusters with many dangling bonds renders them as inadequate for approximating the potential of the bulk of the solid. The unrealistic atomic charges at the center of these clusters (positive net atomic charge on the nitrogen in B_3N) also supports this conclusion. Only sufficiently close to the nuclei ($R \leq 0.3$ a.u.) these potentials reproduce the convergence-limit results due to the increasing contributions of the nuclear potential.

The satisfactory convergence of both the atomic charges and the electrostatic potentials at the center of the clusters employed in the present study, indicates that these clusters might be used to approximate the matrix elements necessary for band-structure calculation. It is indeed found that the largest difference between any given matrix element $[H^{\alpha\delta}_{\mu\nu}(0-n)]$ for $n \leq 2$ as calculated from clusters 6 and 7 did not exceed 0.2% using the CNDO approximation, or 0.4% using the SIEXH calculation, while the largest difference between the results of clusters 5 and 6 were 0.4% and 0.5% for CNDO and SIEXH calculations, respectively. Table IV compares the SIEXH results obtained by using a direct Brillouin-zone integration [Eq. (4)] with those obtained by the cluster band-structure method in which the matrix elements needed in Eq.

TABLE III. Calculated electrostatic potentials (in kcal/mole) at selected points (see Fig. 5) along the central B-N bond in clusters of increasing size. For the numbering of the clusters also see Fig. 5.

Point	Cluster 1	Cluster 2	Cluster 3	Cluster 4	Cluster 5
1	-6.4367×10^{2}	-5.8261×10^{2}	-5.8170×10^{2}	-5.6865×10^{2}	-5.6861×10^{2}
2	-5.4704×10^{4}	-5.4690×10^{4}	-5.4683×10^{4}	-5.4683×10^{4}	-5.4683×10^{4}
3	-8.9978×10^{4}	-9.0074×10^{4}	-9.0076×10^{4}	-9.0076×10^{4}	-9.0076×10^{4}
4	-3.6804×10^{1}	-1.5936×10^{2}	-1.6397×10^{2}	-1.8908×10^{2}	-1.8909×10^{2}
5	-3.0383×10^{2}	-2.2801×10^{2}	-2.6604×10^{4}	-2.6616×10^{2}	-2.6616×10^{2}

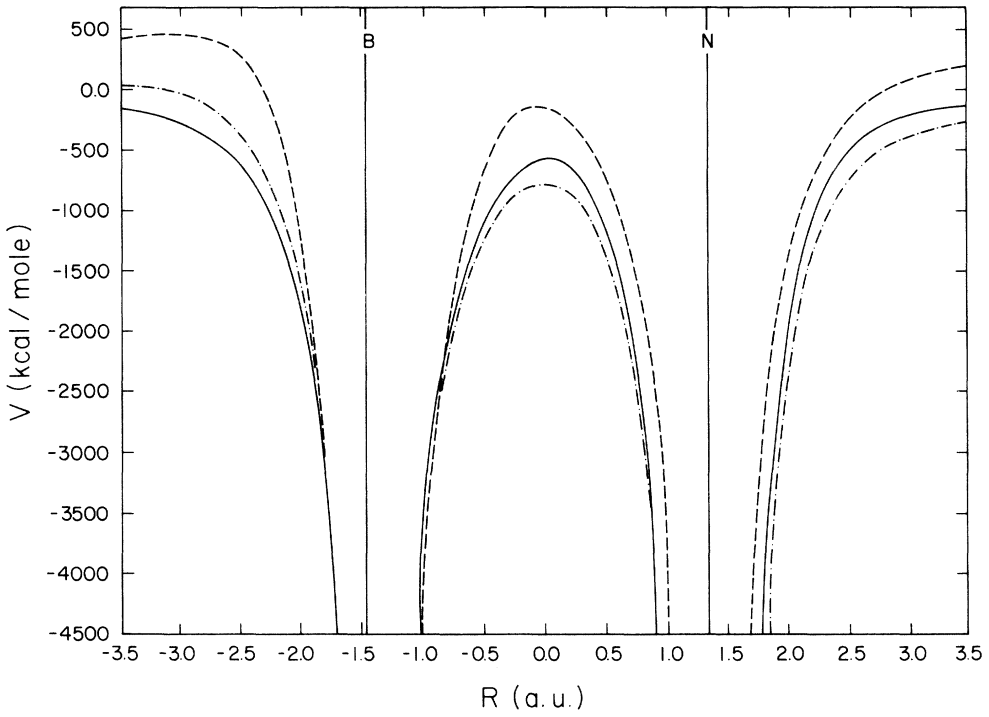

FIG. 8. Electrostatic potentials computed from CNDO charge density for small clusters, along the central B-N bond (Fig. 5). The B-N distance was taken as 1.446 Å. Distance denoted in atomic units. Dashed line, B_3N; solid line, N_3B, dash-dot line, Cluster 7 (Fig. 5).

(3) are computed from the finite clusters. A similar comparison for the CNDO calculations is shown in Table V where the CNDO band structure calculated by Kapsomenos[56] and confirmed by our independent calculation is compared with the CNDO cluster band structure. It is seen that although the CNDO and SIEXH results differ markedly, the results of the cluster band-structure approximate very well those of the direct self-consistent method, in both cases. It thus appears, that it is possible to obtain good approximations to the self-consistent band structure by replacing the "free-atom" potentials used in noniterative tight-binding methods, with the matrix elements obtained from self-consistent-field (SCF) calculations on finite clusters. CNDO band-structure calculations were previously shown to yield very poor results (overestimation of the band widths by a factor of 5–10 and overestimation of the lowest interband transitions by a factor of ~3) both in graphite[56–58], and in boron nitride,[56,58] mainly due to the neglect of overlap. In these covalent systems, characterized by short bonds, the overlap integrals play an essential role in determining the crystal eigenvalue spectrum.[2,59] Thus in further discussions, only the SIEXH and

TABLE IV. Comparison of the results of crystal band structure, cluster band structure, and truncated crystal calculations within the SIEXH approximation. All results given in eV.

Property	SIEXH Crystal band structure	SIEXH Cluster band structure	SIEXH Truncated crystal
Band gap	3.7	3.7	2.95
π bandwidth	1.4	1.3	3.31
Total valence width	18.6	18.5	17.53
$Q_2^- \rightarrow Q_2^-$ $(\pi \rightarrow \pi^*)$	6.0	6.0	5.96
$2S_N$ band minimum	$18.8 + E_F$	$18.6 + E_F$	$18.8 + E_F$

TABLE V. Comparison of the results of crystal band structure and the cluster band structure as calculated from the CNDO approximation. All results given in eV.

Property	CNDO Crystal band structure[56]	CNDO Cluster band structure
Band gap	13.3	12.8
π bandwidth	21.3	20.9
Total bandwidth	47.8	46.9
$Q_2^- \rightarrow Q_2^-$ $(\pi \rightarrow \pi^*)$	17.5	17.3
$2S_N$ band minimum	51.2	50.8

the MIEXH methods will be considered.

In Table IV we have also compared the results of the periodic band-structure calculation with those obtained by the truncated-crystal method.[5] The latter method, used previously in many calculations both with the $X\alpha$-scattered-wave technique[60,61] and with LCAO methods,[5,62-64] approximates the crystalline band structure by the electronic eigenvalue spectrum of finite clusters of atoms arranged according to the known crystal structure. It has been previously indicated[5] that various features of the energy spectrum (bandwidths, band gaps, interband transition energies, etc.) of finite clusters with no periodic boundary conditions, *reveal a nonmonotonic behavior as a function of cluster size*, unless special symmetries are considered. Thus, besides the unphysical charge inhomogeneity associated with the dangling bonds on the clusters surface,[61,62] symmetry considerations might already exclude some significant one-electron energy levels (e.g., those determining the band edges or band gap) from the eigenvalue spectrum of improperly chosen small clusters. It has been shown for instance, that in two-dimensional hexagonal structures, finite clusters having m full hexagons in the x direction and n full hexagons in the y direction, will always exhibit some one-electron levels that will transform according to the representations of the Q point in the infinite crystal, while levels transforming like the P-point representations do not occur in finite clusters. Thus, while the interband transitions at the Q point are reasonably approximated by truncated clusters such as cluster 6 (Table IV), the band gap is underestimated by such a cluster. Bandwidths involving differences between one-electron levels where at least one of them is a P-type level, (e.g., the π bandwidth $W_\pi = \mathcal{E}_{P_1^-} - \mathcal{E}_{\Gamma_2^-}$) or the total valence width ($W_{\text{tot}} = \mathcal{E}_{P_1^-} - \mathcal{E}_{\Gamma_1^-}$) are similarly underestimated by truncated cluster models and many more atoms should be included to obtain reliable estimates. A similar behavior of the truncated crystal results relative to periodic band-structure results, have been obtained by Messmer and Watkins[65] for diamond. It thus seems that unless very large truncated clusters are to be employed the electronic properties of the regular lattice are better obtained by using the latter approach to extract the self-consistent matrix elements to be used in periodic band-structure calculations.

We now turn to examine the effect of the self-consistency requirement on the crystal potential. We have computed the LCAO wave functions of the largest cluster employed (cluster 7 in Fig. 5) under various energy convergence criteria ΔE (denoting the largest allowed difference in the total electronic energy in the last two successive iterations). The resulting wave functions of the occupied levels were used to compute the electronic density and the electrostatic potential was then calculated according to Eqs. (13)–(15). It is seen from Table VI that as the degree of self-consistency increases (ΔE decreases), the potential at the center of the B-N bond (denoted in Fig. 5 as point 1) and close to the center of the neighboring hexagons (points 4, 5) undergo substantial changes, while close to the nuclei (points 2, 3) the effect is smaller due to the high contributions from the constant nuclear potential. This tendency is also reflected in the computed values of the π bond orders of the B-N bond; this value decreases from 0.4911 at $\Delta E \sim 10^{-1}$ a.u. to 0.4882 at $\Delta E \sim 10^{-5}$ a.u. The accompanying changes in the band structure are very pronounced (e.g. the band gap changes from 3.7 eV in the iterated calculation to 5.8 eV in the uniterated calculation) being of the same order of magnitude obtained previously in self-consistent versus non-self-consistent OPW calculations on II–VI crystals.[31]

V. CONCLUSIONS

The absorption spectrum of the hexagonal boron nitride sample (Fig. 1) exhibits its main peak at 6.2 eV and shows a sharp drop at 5.8 eV. The peak is assigned to the lowest Q-saddle point transition $Q_2^- \rightarrow Q_2^-$ between the π bands while the onset of the transition at 5.8 eV is assigned to the direct $\pi \rightarrow \pi^*$ gap at $P_1^- \rightarrow P_2^-$. The reflectivity spectrum (Fig. 3) also indicates that $E_g > 5$ eV. It seems therefore that the low values for the gap reported in earlier publications (see Introduction) do not correspond to the gap. These low values for E_g were obtained from comparatively thick films which limited the spectral range of the absorption measurements to below about 5.0–5.5 eV. Under these conditions only the shoulder in the range was observed. The optical data obtained in the present study agree favorably with the calculated results

TABLE VI. Effect of self-consistency on the electrostatic potential along the path denoted in Fig. 1 (see also for numbering of points). The calculations are performed on the largest cluster used (Cluster 7, Fig. 1). ΔE denotes the energy convergence criterion imposed on each SCF calculation.

Point	V (kcal/mole) $\Delta E \leq 10^{-1}$ a.u.	V (kcal/mole) $\Delta E \leq 10^{-2}$ a.u.	V (kcal/mole) $\Delta E \leq 10^{-5}$ a.u.
1	-5.942×10^{2}	-5.711×10^{2}	-5.686×10^{2}
2	-5.474×10^{4}	-5.470×10^{4}	-5.469×10^{4}
3	-9.007×10^{4}	-9.006×10^{4}	-9.005×10^{4}
4	-2.676×10^{4}	-2.588×10^{2}	-2.565×10^{4}
5	-2.013×10^{2}	-1.912×10^{2}	-1.891×10^{4}

using the modified iterative extended Hückel (MIEXH) method. It should also be noted that reflection measurements indicated[9] that $E_g > 5.5$ eV and showed[10] a prominant peak at 6.2 eV which fits well the results of the present work. In addition, photoconductivity measurement in the present work (Fig. 4) as well as glow-curve measurements[66] also indicate $E_g > 4.5$ eV. We conclude therefore that the "knee" in the absorption spectrum near 4 eV does not correspond to the gap of the pure crystal.

The experimental temperature dependence of the band gap fitted to the expression $E_g(T) = E_g(0) - \beta T$ reveals a very low-temperature coefficient ($\beta < 4 \times 10^{-5}$ eV/°K). This value is lower by at least an order of magnitude compared to shifts in cubic III-V compounds. This abnormally low value is explained theoretically by the absence of the two-center boron-nitrogen terms in the expression for the gap due to the special symmetry of the P-point in the hexagonal Brillouin zone.

The main conclusions to be made from the theoretical study in this work can be summarized as follows:

(i) Owing to the substantial electronegativity difference characterizing the atoms constituting the unit cell of the III-V compounds, significant charge redistribution occurs in the solid, resulting in a modification in the electrostatic potential, bond orders, etc. A charge self-consistent calculation is thus essential for a proper description of the electronic properties. Simple noniterative schemes (e.g., extended Hückel, conventional tight binding) based on neutral atom potentials, grossly overestimate the ionicity of the structure and the polarity of the charge distribution.

(ii) Iterative schemes using only one-center terms linear in the net charges (e.g., simple iterative extended Hückel) tend to overestimate the charge neutrality of the system and the charge dependence of the interaction matrix elements due to the absence of binding effects to oppose the homogenization process. This results in low gaps and relatively narrow bands. Introduction of Madelung-type two-center terms (e.g., in modified iterative extended Hückel scheme) reduces the charge dependence of the various matrix elements through near cancellation with the one-center terms. The modified elements resemble somewhat those of the non-self-consistent approach in their low-charge dependence, however, it is this residual dependence that accounts for the proper charge redistribution in the system.

(iii) In a highly covalent system like boron nitride it is possible to obtain the self-consistent matrix elements needed in the band-structure calculation, from the SCF-LCAO solutions of finite clusters of atoms. The convergence of the matrix elements relating atoms that are at the *center* of the cluster is examined as a function of the cluster's size. The electrostatic Poisson potential across the cluster, computed from the LCAO charge density, is used as a monitor to the degree of perturbation exerted by the dangling bonds on the center of the cluster. Since the covalent bonding in such systems is determined mainly by the electronic charge distribution at the vicinity of the bond, such a procedure converges rather rapidly and medium-size clusters surrounding a given B-N bond already yield satisfactory values for the matrix elements associated with that bond.

(iv) Simple truncated crystal models approximating the band structure of the infinite solid by the energy eigenvalue spectrum of finite clusters should be carefully selected due to the nonmonotonic behavior of various electronic properties as a function of the cluster's size. Only clusters with specially chosen symmetries could be used to obtain some of the one-electron energy levels that correspond to high-symmetry points in the crystal (e.g., those determining band gaps and bandwidths).

(v) Though the semiempirical LCAO methods that have been previously used for studying molecular properties, constitute only approximation to the exact Hartree-Fock scheme, they provide a simple and practical means for obtaining a rather physical description of electronic properties of solids. The basic solid-state features concerning charge redistribution, ionicity, band structure and density of states are amenable to a relatively simple treatment by these methods. It should however be stressed that extreme caution should be experienced in examining the adequacy of the various quantum-chemical approximations to solids, regarding the effects introduced by the neglect of overlap interaction and self-consistency.

ACKNOWLEDGMENTS

The authors wish to thank Dr. Baronian for supplying the samples used in this work, and Dr. O. Naveh who carried out the reflectance measurements.

*Present address: Department of Physics, Northwestern University, Evanston, Illinois 60201.

[1]R. Taylor and C. A. Coulson, Proc. Phys. Soc. Lond. A 65, 834 (1952).

[2]E. Doni and G. P. Parravicini, Nuovo Cimento A 63, 117 (1969).

[3]J. Zupan, Phys. Rev. B 6, 2477 (1972).

[4]M. S. Nakhmanson and V. P. Smirnov, Fiz. Tverd. Tela 13, 3788 (1971) [Sov. Phys.-Solid State 13, 752 (1971); and 13, 2763 (1972)].

[5]A. Zunger, J. Phys. C 6, 76 (1974); 6, 96 (1974).
[6]V. A. Fomichev, Fiz. Tverd. Tela 13, 907 (1971) [Sov. Phys.-Solid State 13, 754 (1971)].
[7]K. Hamrin, G. Johansson, U. Gelius, C. Nordling, and K. Siegbahn, Phys. Scr. 1, 277 (1970).
[8]R. Vilanove, C. R. Acad. Sci. B 272, 1066 (1971).
[9]S. Larach and R. E. Shrader, Phys. Rev. 104, 68 (1956).
[10]W. J. Choyke (private communication cited in Ref. 2).
[11]M. J. Rand and J. F. Roberts, J. Electrochem. Soc. 115, 423 (1968).
[12]A. J. Noreika and M. H. Francombe, J. Vac. Sci. Technol. 6, 722 (1969).
[13]W. Baronian, Mater. Res. Bull. 7, 119 (1972).
[14]J. Zupan and D. Kolar, J. Phys. C 5, 3097 (1972).
[15]Y. Yacob and O. Naveh, Phys. Rev. B 7, 3991 (1973).
[16]O. Madelung, *Physics of* III-V *Compounds* (Wiley, New York, 1964), p. 36.
[17]The refractive index n and the extinction coefficient $k=(\lambda/4\pi)K$ of thin films can be deduced (see Ref. 18) from measurements of T and R. We were not able to use this procedure, since our reflectivity measurements setup was limited to wavelengths above 2300 Å.
[18]J. F. Hall, J. Opt. Soc. Am. 46, 1013 (1956).
[19](a) R. Hoffman, J. Chem. Phys. 39, 1397 (1963); (b) 40, 2474 (1964).
[20]M. A. Skinner and H. O. Pritchard, Trans. Faraday Soc. 49, 1254 (1953); and Chem. Rev. 55, 745 (1955).
[21]G. Blyholder and C. A. Coulson, Theor. Chim. Acta 10, 316 (1968).
[22]T. L. Gilbert in *Sigma Molecular Orbital Theory*, edited by O. Sinanoğlu and R. Wiberg (Yale U.P., New Haven, 1970), p. 349.
[23]R. Rein, H. Fukuda, H. Win, G. A. Clark, and F. E. Harris, in *Proceedings of the Jerusalem Symposium* edited by A. Pullman and E. Bergman (Israel Academy of Science and Humanities, Jerusalem, 1969), p. 86.
[24]R. Rein, H. Fukuda, H. Win, and G. A. Clark, J. Chem. Phys. 45, 4743 (1966).
[25]L. C. Cusachs, J. Chem. Phys. 43, S157 (1965).
[26]L. C. Cusachs and J. W. Reynolds, J. Chem. Phys. 43, S 160 (1965).
[27]R. S. Mulliken, J. Chem. Phys. 23, 433 (1955).
[28]J. A. Pople and D. L. Beveridge, *Approximate M. O. Theory* (McGraw-Hill, New York, 1970).
[29]N. Mataga, Bull. Chem. Soc. Jpn. 31, 453 (1958).
[30]W. E. Rudge, Phys. Rev. 181, 1024, 1033 (1969).
[31]D. J. Stukel, R. N. Euwema, and T. C. Collins, Phys. Rev. 179, 740 (1969).
[32]D. L. Beveridge, J. Jano, and J. Ludik, J. Chem. Phys. 56, 4744 (1972).
[33]J. M. Andrè, J. Chem. Phys. 50, 1536 (1969).
[34]C. A. Coulson and R. Taylor, Proc. Phys. Soc. Lond. A 65, 815 (1952).
[35]R. Taylor and C. A. Coulson, Proc. Phys. Soc. Lond. A 65, 834 (1952).
[36]R. S. Pease, Acta. Crystallogr. 5, 356 (1952).
[37]G. Giessnen-Perttre and A. Pullman, Theor. Chim. Acta 25, 83 (1972); C. R. Acad. Sci. (Paris) C 272, 750 (1972).
[38]S. Srebrenic, H. Weinstein, and R. Pauncz, Chem. Phys. Lett. 20, 419 (1973).
[39]W. J. Hehre, R. F. Steward, and J. A. Pople, J. Chem. Phys. 51, 2657 (1969).
[40]M. J. Cazaux, C. R. Acad. Sci. B 270, 700 (1970).
[41]D. L. Greenaway, G. Harbeke, F. Bassani, and E. Tosatti, Phys. Rev. 178, 1340 (1969).
[42]G. S. Painter and D. E. Ellis, Phys. Rev. B 1, 4747 (1970).
[43]R. F. Willis, B. Feuerbacher, and B. Fitton, Phys. Rev. B 8, 2441 (1971).
[44]S. D. Peyerimhoff and R. J. Buenker, Theor. Chim. Acta 19, 1 (1970).
[45]H. Bock and W. Fuss, Angew. Chem. 83, 169 (1971).
[46]M. B. Khusidman, Fiz. Tverd. Tela 14, 3287 (1972) [Sov. Phys.-Solid State 14, 2791 (1973)].
[47]A. Zunger and A. Katzir, Phys. Rev. B 11, 2378 (1975).
[48]C. K. Jorgensen, S. M. Horner, W. E. Hatfield, and S. Y. Tyree, Int. J. Quantum Chem. 1, 191 (1967).
[49]K. S. Wheelock, H. B. Jonassen, and L. C. Cusachs, Int. J. Quantum Chem. 4, 209 (1971).
[50]F. Bassani and M. Yoshimine, Phys. Rev. 130, 20 (1963).
[51]R. M. Chrenko, Solid State Commun. 14, 511 (1974).
[52]J. C. Phillips and J. A. Van Vechten, Phys. Rev. B 2, 2147 (1970).
[53]J. C. Phillips, Rev. Mod. Phys. 42, 317 (1970).
[54]R. H. Bube, *Photoconductivity in Solids* (Wiley, New York, 1960).
[55]A. Zunger, Solid State Commun. 11, 1727 (1972).
[56]G. Kapsomenos, Ph.D. thesis (University Catholique de Louvain, 1972) (unpublished).
[57]A. J. Bennett, B. McCarrol, and R. P. Messmer, Surf. Sci. 24, 191 (1967).
[58]A. Zunger and R. Englman (unpublished).
[59]W. M. Lomer, Proc. R. Soc. A 227, 330 (1955).
[60]K. H. Johnson, J. G. Norman, and J. W. D. Connolly, in *Computational Methods for Large Molecules and Localized States in Solids*, edited by F. Herman, A. D. McLean, and R. K. Nesbet (Plenum, New York, 1973), p. 161.
[61]G. D. Watkins and R. P. Messmer, Phys. Rev. Lett. 32, 1244 (1974).
[62]F. P. Larkins, J. Phys. C 4, 3065 (1971); 4, 3077 (1971).
[63]R. P. Messmer and G. D. Watkins, Phys. Rev. Lett. 25, 656 (1970).
[64]A. Zunger, J. Phys. Chem. Solids 36, 229 (1975).
[65]R. P. Messmer and G. D. Watkins, Phys. Rev. B 7, 2568 (1973).
[66]A. Katzir, J. T. Suss, A. Zunger, and A. Halperin, Phys. Rev. B 11, 2370 (1975).